On shape coexistence and possible shape isomers of nuclei around ^{172}Hg[*]

Xin Guan,[1,†] Jing Guo,[1] Qi-Wen Sun,[1] Bożena Nerlo-Pomorska,[2] and Krzysztof Pomorski[2]

[1]*Department of Physics, Liaoning Normal University, Dalian 116029, China*
[2]*Institute of Physics, Maria Curie Skłodowska University, 20-031 Lublin, Poland*

This study explores the phenomenon of shape coexistence in nuclei around ^{172}Hg, with a focus on the isotopes ^{170}Pt, ^{172}Hg, and ^{174}Pb, as well as the ^{170}Pt to ^{180}Pt isotopic chain. Utilizing a macroscopic-microscopic approach that incorporates the Lublin-Strasbourg Drop model combined with a Yukawa-Folded potential and pairing corrections, we analyze the potential energy surfaces (PES) to understand the impact of pairing interaction.

For ^{170}Pt, the PES shows a prolate ground-state, with additional triaxial and oblate shape isomers. In ^{172}Hg, the ground-state deformation transitions from triaxial to oblate with increasing pairing interaction, demonstrating its nearly γ-unstable nature. Three shape isomers (prolate, triaxial, and oblate) are observed, with increasing pairing strength leading to the disappearance of the triaxial isomer. ^{174}Pb exhibits a prolate ground-state that becomes increasingly spherical with stronger pairing, and while shape isomers are present at lower pairing strengths, robust shape coexistence is not observed. For realistic pairing interaction, the ground-state shapes transition from prolate in ^{170}Pt to a coexistence of γ-unstable and oblate shapes in ^{172}Hg, ultimately approaching spherical symmetry in ^{174}Pb. The comparison between Exact and BCS pairing demonstrates that BCS pairing tends to smooth out shape coexistence and reduce the depth of shape isomer, leading to less pronounced deformation features.

The potential energy surfaces (PES) for even-even $^{170-180}$Pt isotopes reveal significant shape evolution. ^{170}Pt shows a prolate ground-state, while ^{172}Pt exhibits triaxial and prolate shape coexistence. In ^{174}Pt, the ground-state is triaxial, coexisting with a prolate minimum. For ^{176}Pt, a γ-unstable ground-state coexists with a prolate minimum. By ^{178}Pt and ^{180}Pt, a dominant prolate minimum emerges. These results highlight the role of shape coexistence and γ-instability in the evolution of nuclear structure, especially in the mid-shell region.

These findings highlight the importance of pairing interactions in nuclear deformation and shape coexistence, providing insights into the structural evolution of mid-shell nuclei.

Keywords: Macro-micro model, Shape coexistence, Shape isomers, Exact and BCS pairing solutions

I. INTRODUCTION

The phenomenon of shape coexistence in atomic nuclei has garnered significant attention in the field of nuclear physics and has become a prominent topic in contemporary research. This phenomenon refers to the presence of multiple distinct shapes within a single nucleus, where states with similar energies exhibit different deformations [1]. Understanding nuclear shapes is crucial for revealing the internal structure and properties of nuclei, providing tools for predicting and explaining nuclear behaviors, and advancing nuclear physics.

The study of nuclear shapes can be traced back to Haruhiko Morinaga's 1956 paper [2], which explained the properties of the first excited state and ground state of ^{16}O, introducing the concept of multi-nucleon cross-shell excitation to describe deformation characteristics. Over the past five decades, shape coexistence has evolved from a rare phenomenon to a common feature observed in many nuclei, highlighting its significance in nuclear structure research [3]. Recent experimental studies have revealed significant evidence of shape coexistence phenomena in neutron-deficient isotopes of lead and mercury. For instance, the study [4] specifically focuses on the ^{188}Hg isotope, where theoretical predictions suggest the presence of shape coexistence.

These findings have led to increased theoretical investigations into nuclear shape coexistence, utilizing advanced experimental techniques such as tagging techniques at the University of Jyväskylä, Coulomb-excitation experiments at CERN, and relativistic energy-fragmentation experiments at GSI [5]. These experiments underscore the importance of understanding the mechanisms that govern nuclear shape evolution. Building upon these experimental insights, theoretical investigations have played a pivotal role in elucidating the complexities of shape coexistence [6–8]. Previous studies have employed various theoretical frameworks, including macroscopic-microscopic approaches and self-consistent models, to perform comprehensive calculations of nuclear ground-state masses and deformations across a wide range of nuclei [3].

Despite its success, the Bardeen-Cooper-Schrieffer (BCS) method [9] and the more refined Hartree-Fock-Bogolyubov (HFB) approach face limitations due to the small number of valence nucleons under the pairing correlation's influence [10–12]. These methods often fail to conserve particle numbers, leading to inaccuracies in describing higher-lying excited states [13]. Alternatives such as the shell model provide successful descriptions but are limited by the combinatorial growth of model space sizes, necessitating truncation schemes for heavy nuclei and often being constrained by computational resources [14].

The exact solution to the standard pairing problem, first obtained by Richardson and now referred to as the Richardson-Gaudin method, offers a promising approach for a micro-

* Supported by the National Natural Science Foundation of China (No.12275115,12175097).
† Corresponding author, Xin Guan, guanxin@lnnu.edu.cn.

scopic treatment of clustering in heavy nuclei [15–18]. This method is particularly suitable for handling the large model spaces and the pairing and shell effects necessary for accurately describing heavy nuclei [19–22]. In our previous work, the deformed mean-field plus pairing model within the Richardson-Gaudin method was used to explore the quantum phase transition around neutron number $N \sim 90$ in the $A \sim 150$ mass region [23]. The analysis demonstrated the critical behavior of the shape phase transition driven by the competition between deformation and pairing interactions. More recently, a new iterative algorithm has been developed to find the exact solution to the standard pairing problem within the Richardson-Gaudin method [24], which has shown excellent agreement with experimental data when applied to actinide fission nuclei isotopes [25–27]. Recently, K. Pomorski et al., using the Lublin-Strasbourg Drop (LSD) with a Yukawa-Folded single-particle potential, plus the BCS pairing correction in a macroscopic-microscopic model, provided the deformation potential energy surfaces of nuclei near $Z = 82$. This study investigated the shape coexistence phenomenon in even-even isotopes of Pt, Hg, and Pb [28].

The aim of the current paper is to extend this line of inquiry by presenting a systematic study of potential energy surfaces for even-even Pt, Hg, and Pb isotopes near $Z = 82$. Our investigation leverages recent advancements in shape parametrization and adopts a macroscopic-microscopic approach, integrating the Lublin-Strasbourg Drop (LSD) model with a Yukawa-Folded single-particle potential. The analysis focuses on the impact of pairing interactions on the shape coexistence of the ^{170}Pt, ^{172}Hg, ^{174}Pb nuclei, as well as the $^{170-180}$Pt even-even isotopes.

II. THEORETICAL FRAMEWORK AND NUMERICAL DETAILS

A. Deformed mean-field plus standard pairing model

The Hamiltonian of the deformed mean-field plus standard pairing model for either the proton or the neutron sector is given by

$$\hat{H} = \sum_{i=1}^{n} \varepsilon_i \hat{n}_i - G \sum_{ii'} S_i^+ S_{i'}^-, \tag{1}$$

where the sums run over all given i-double degeneracy levels of total number n, $G > 0$ is the overall pairing interaction strength, $\{\varepsilon_i\}$ are the single-particle energies obtained from mean-field, such as Hartree-Fock (HF), Woods-Saxon potential (WS), Yukawa-Folded (YF)single-particle potential, or Nilsson model. $n_i = a_{i\uparrow}^\dagger a_{i\uparrow} + a_{i\downarrow}^\dagger a_{i\downarrow}$ is the fermion number operator for the i-th double degeneracy level, and $S_i^+ = a_{i\uparrow}^\dagger a_{i\downarrow}^\dagger$ $[S_i^- = (S_i^+)^\dagger = a_{i\downarrow} a_{i\uparrow}]$ is the pair creation (annihilation) operator, The up and down arrows in these expressions refer to time-reversed states.

According to the Richardson-Gaudin method [15–18], the exact k-pair eigenstates of (1) with $\nu_{i'} = 0$ for even systems or $\nu_{i'} = 1$ for odd systems, in which i' is the label of the double degeneracy level that is occupied by an unpaired single particle can be written as

$$|k;\xi;\nu_{i'}\rangle = S^+(x_1^{(\xi)}) S^+(x_2^{(\xi)}) \cdots S^+(x_k^{(\xi)}) |\nu_{i'}\rangle, \tag{2}$$

where $|\nu_{i'}\rangle$ is the pairing vacuum state with the seniority $\nu_{i'}$ that satisfies $S_i^- |\nu_{i'}\rangle = 0$ and $\hat{n}_i |\nu_{i'}\rangle = \delta_{ii'} \nu_i |\nu_{i'}\rangle$ for all i. Here, ξ is an additional quantum number for distinguishing different eigenvectors with the same quantum number k and

$$S^+(x_\mu^{(\xi)}) = \sum_{i=1}^{n} \frac{1}{x_\mu^{(\xi)} - 2\varepsilon_i} S_i^+, \tag{3}$$

in which the spectral parameters $x_\mu^{(\xi)}$ $(\mu = 1, 2, \ldots, k)$ satisfy the following set of Bethe ansatz equations (BAEs):

$$1 + G \sum_i \frac{\Omega_i}{x_\mu^{(\xi)} - 2\varepsilon_i} - 2G \sum_{\mu'=1(\neq\mu)}^{k} \frac{1}{x_\mu^{(\xi)} - x_{\mu'}^{(\xi)}} = 0, \tag{4}$$

where the first sum runs over all i levels and $\Omega_i = 1 - \delta_{ii'} \nu_{i'}$. For each solution, the corresponding eigenenergy is given by

$$E_k^{(\xi)} = \sum_{\mu=1}^{k} x_\mu^{(\xi)} + \nu_{i'} \varepsilon_{i'}. \tag{5}$$

In general, according to the polynomial approach in Refs. [20–22], one can find solutions of Eq. (4) by solving the second-order Fuchsian equation [19] as

$$A(x) P''(x) + B(x) P'(x) - V(x) P(x) = 0, \tag{6}$$

where $A(x) = \prod_{i=1}^{n} (x_\mu^{(\xi)} - 2\varepsilon_i)$ is an n-degree polynomial,

$$B(x)/A(x) = -\sum_{i=1}^{n} \frac{\Omega_i}{x_\mu^{(\xi)} - 2\varepsilon_i} - \frac{1}{G}, \tag{7}$$

$V(x)$ are called Van Vleck polynomials [19] of degree $n-1$, which are determined according to Eq. (6). They are defined as

$$V(x) = \sum_{i=0}^{n-1} b_i x^i. \tag{8}$$

The polynomials $P(x)$ with zeros corresponding to the solutions of Eq. (4) is defined as

$$P(x) = \prod_{i=1}^{k} (x - x_i^{(\xi)}) = \sum_{i=0}^{k} a_i x^i, \tag{9}$$

where k is the number of pairs. b_i and a_i are the expansion coefficients to be determined instead of the Richardson variables x_i. Furthermore, if we set $a_k = 1$ in $P(x)$, the coefficient a_{k-1} then equals the negative sum of the $P(x)$ zeros, $a_{k-1} = -\sum_{i=1}^{k} x_i^{(\xi)} = -E_k^{(\xi)}$.

If the value of x approaches twice the single-particle energy of a given level δ, i.e., $x = 2\varepsilon_\delta$, one can rewrite Eq. (6) in doubly degenerate systems with $\Omega_i = 1$ as [20, 22]

$$\left(\frac{P'(2\varepsilon_\delta)}{P(2\varepsilon_\delta)}\right)^2 - \frac{1}{G}\left(\frac{P'(2\varepsilon_\delta)}{P(2\varepsilon_\delta)}\right) = \sum_{i\neq\delta} \frac{\left[\left(\frac{P'(2\varepsilon_\delta)}{P(2\varepsilon_\delta)}\right) - \left(\frac{P'(2\varepsilon_i)}{P(2\varepsilon_i)}\right)\right]}{2\varepsilon_\delta - 2\varepsilon_i} \quad (10)$$

In Ref. [24], a new iterative algorithm is established for the exact solution of the standard pairing problem within the Richardson-Gaudin method using the polynomial approach in Eq. (10). It provides efficient and robust solutions for both spherical and deformed systems at a large scale. The key to its success is determining the initial guesses for the large-set nonlinear equations involved in a controllable and physically motivated manner. Moreover, one reduces the large-dimensional problem to a one-dimensional Monte Carlo sampling procedure, which improves the algorithm's efficiency and avoids the nonsolutions and numerical instabilities that persist in most existing approaches. Based on the new iterative algorithm, we applied the model to study the actinide nuclei isotopes, where an excellent agreement with experimental data was obtained [24–27].

B. The Fourier shape parametrization

Recent studies have demonstrated that the developed Fourier parametrization of deformed nuclear shapes is highly effective in capturing the essential features of nuclear shapes, particularly up to the scission configuration [28, 29]. Current research indicates that combining this innovative Fourier shape parametrization with the LSD + Yukawa-Folded macroscopic-microscopic potential-energy framework is exceptionally efficient [26, 27, 30, 31]. This work primarily adopts the macroscopic-microscopic framework outlined in Refs. [26, 27], where the single-particle energies $\{\epsilon_i\}$ in the model Hamiltonian (1) are derived from the Yukawa-Folded potential.

The nuclear surface is expanded in terms of a Fourier series of dimensionless coordinates as follows:

$$\frac{\rho_s^2(z)}{R_0^2} = \sum_{n=1}^{\infty}\left[a_{2n}\cos\left(\frac{(2n-1)\pi}{2}\frac{z-z_{\rm sh}}{z_0}\right)\right.$$
$$\left.+a_{2n+1}\sin\left(\frac{2n\pi}{2}\frac{z-z_{\rm sh}}{z_0}\right)\right], \quad (11)$$

where $\rho_s(z)$ is the distance from a surface point to the symmetry z-axis, and $R_0 = 1.2A^{1/3}$ fm is the radius of a corresponding spherical shape with the same volume. The shape's extension along the symmetry axis is $2z_0$, with the left and right ends located at $z_{\rm min} = z_{\rm sh} - z_0$ and $z_{\rm max} = z_{\rm sh} + z_0$, respectively. The parameter z_0 represents half the shape's extension along the symmetry axis and is determined by volume conservation, while $z_{\rm sh}$ is set such that the center of mass of the nuclear shape is at the origin of the coordinate system. Based on the convergence properties discussed in Ref. [28], the first five terms $a_2, \ldots, a_6$ are retained as a starting point, and the parameters a_n are transformed into deformation parameters q_n as follows:

$$\begin{aligned}
q_2 &= a_2^{(0)}/a_2 - a_2/a_2^{(0)},\\
q_3 &= a_3,\\
q_4 &= a_4 + \sqrt{(q_2/9)^2 + (a_4^{(0)})^2},\\
q_5 &= a_5 - (q_2-2)a_3/10,\\
q_6 &= a_6 - \sqrt{(q_2/100)^2 + (a_6^{(0)})^2},
\end{aligned} \quad (12)$$

where $a_n^{(0)}$ are the Fourier coefficients for the spherical shape. Higher-order coordinates q_5 and q_6 are generally set to zero within the accuracy of the current approach. The set of q_i parameters has explicit physical significance in describing the shape of the fissioning nucleus: q_2 denotes the elongation, q_4 represents the neck parameter, and q_3 indicates the left-right asymmetry.

Additionally, the non-axial deformation of nuclear shapes is described as follows, assuming that the surface cross-section at a given z-coordinate is elliptical with semi-axes $a(z)$ and $b(z)$:

$$\varrho_s^2(z,\varphi) = \rho_s^2(z)\frac{1-\eta^2}{1+\eta^2+2\eta\cos(2\varphi)}, \quad (13)$$

where $\eta = \frac{b-a}{b+a}$ characterizes the non-axial deformation. Volume conservation requires that $\rho_s^2(z) = a(z) + b(z)$, with the condition $ab = \rho_s^2(z)$ ensuring volume conservation for non-axial deformations. The semi-axes are then given by:

$$a(z) = \rho_s(z)\sqrt{\frac{1-\eta}{1+\eta}}, \quad b(z) = \rho_s(z)\sqrt{\frac{1+\eta}{1-\eta}}, \quad (14)$$

This description of non-axial shapes using the parameters q_2 and η is more general than the commonly used Bohr parametrization (β,γ). For spheroidal shapes, both descriptions are equivalent. However, as shown in Fig. 1, where the two parametrizations are compared, the periodicity of nuclear shapes by a 60° rotation angle is similar in both (q_2,η) and (β,γ) planes. It is important to note that this regularity is disrupted when higher multipolarity deformations q_n $(n>2)$ are considered, making the $(\eta, q_2, q_3, q_4, q_6)$ shape parametrization substantially more general than the 3-dimensional $(\epsilon_2, \epsilon_4(\gamma), \gamma)$ parametrization used in Ref. [34, 35]. The two parametrizations coincide only in the special case of spheroidal shapes.

It is essential to stress that different points in the (β,γ) and (q_2,η) planes can correspond to identical shapes when higher q_n $(n>2)$ degrees of freedom are neglected, differing only in the interchange of coordinate system axes. For example, the point $(\beta = 0.4, \gamma = 0)$ corresponds to $(q_2 = 0.42, \eta = 0)$ in the new parametrization, representing the same shape as $(\beta = 0.4, \gamma = 120°)$, which corresponds to $(q_2 = -0.21, \eta = 0.16)$ in the new parametrization.

When analyzing potential energy landscapes that include triaxial degrees of freedom, it is crucial to avoid treating as distinct configurations points in the (q_2, η) deformation plane that are merely rotational images of each other at $\gamma = 60°$.

In this study, the dynamic process of nuclear fission will be described in the three-dimensional deformation space (η, q_2, q_4) using the Fourier shape parametrization.

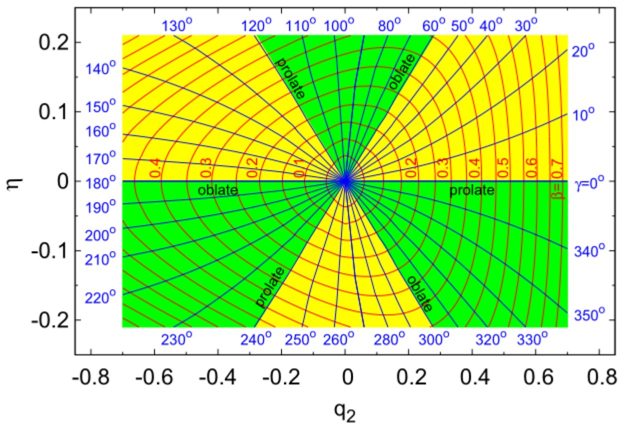

Fig. 1. Relationsheep between the elongation parameter q_2 and the nonaxiality parameter η [28, 29], and the traditional Bohr deformation parameters β and γ is taken from [32, 33]

C. The potential energy

This study calculates the potential energy surfaces (PES) for the isotopes ^{170}Pt, ^{172}Hg, and ^{174}Pb in a three-dimensional deformation space (η, q_2, q_4) and analyzes the impact of pairing interactions on the shape coexistence of these isotopes. The results were obtained over the following grid points in the deformation parameter space:

$$\begin{aligned} \eta &\in [0.00, 0.20] & \Delta\eta &= 0.02 \\ q_2 &\in [-0.60, 0.85] & \Delta q_2 &= 0.05 \\ q_4 &\in [-0.30, 0.30] & \Delta q_4 &= 0.03, \end{aligned} \tag{15}$$

As indicated in the literature [28], the q_3 degree of freedom has no significant impact on the description of shape coexistence for the isotopes discussed in this paper. Therefore, in this study, q_3 is set to 0, and for each point on the PES, q_4 is minimized to find the energy extremum. The potential energy of the system is calculated within the macroscopic-microscopic approach in this work. The total energy $E_{\rm total}(N, Z, q_n)$ of a nucleus with a given deformation is calculated as

$$E_{\rm total}(N, Z, q_n) = E_{\rm LD}(N, Z, q_n) + E_{\rm B}(N, Z, q_n), \tag{16}$$

where $E_{\rm LD}(N, Z, q_n)$ is the macroscopic term approximated by the standard liquid drop model with proton number Z and neutron number N [36]. In the current calculation for the potential-energy surface, we just consider the energy $E_{\rm B}(N, Z, q_n)$ related to the shape parameter $\{q_2, q_4\}$.

$$E_{\rm B}(N, Z, q_n) = E_{\rm shell}(N, Z, q_n) + E_{\rm pair}(N, Z, q_n), \tag{17}$$

The microscopic term consists of the shell correction energy $E^{\nu(\pi)}_{\rm shell}(N, Z, \{\varepsilon_i\}, q_2, q_4)$ proposed by Strutinsky [37, 38] and the pairing interaction energy $E^{\nu(\pi)}_{\rm pair}(N, Z, \{\varepsilon_i\}, q_2, q_4)$ calculated from Eq. (19). Here, ν (π) is the label of the neutron (proton) sector. In the current study, we consider 18 deformed harmonic-oscillator shells in YF single-particle potential to obtain single-particle levels for the microscopic calculations. For the pairing correction energy, we perform 29 single-particle levels around the neutron Fermi level and 22 single-particle levels around the proton Fermi level.

To validate our results and further explore the efficacy of the exactly solvable pairing model, we also calculated the PES for the isotopes considered under the BCS approximation. The pairing correction is determined as the difference between the BCS energy [9] and the single-particle energy sum and the average pairing energy [39].

$$E_{\rm pair} = E_{\rm BCS} - \sum_{i=1}^{k} \varepsilon_i - \widetilde{E}_{\rm pair}, \tag{18}$$

In the BCS approximation the ground-state energy of a system with an even number of particles and a monopole pairing force is given by

$$E_{\rm BCS} = \sum_{i=1}^{k} 2\varepsilon_i v_k^2 - G\left(\sum_{i=1}^{k} u_i v_i\right)^2 - G\sum_{i=1}^{k} v_i^4, \tag{19}$$

where the sums run over the pairs of single-particle states contained in the pairing window defined below. The coefficients v_i and $u_i = \sqrt{1 - v_i^2}$ are the BCS occupation amplitudes.

The average projected pairing energy, for a pairing window of width 2Ω, which is symmetric in energy with respect to the Fermi energy, is equal to

$$\begin{aligned} \widetilde{E}_{pair} = &-\frac{1}{2}\tilde{g}\tilde{\Delta}^2 + \frac{1}{2}\tilde{g}G\tilde{\Delta}\arctan\left(\frac{\Omega}{\tilde{\Delta}}\right) - \log\left(\frac{\Omega}{\tilde{\Delta}}\right)\tilde{\Delta} \\ &+ \frac{3}{4}G\frac{\Omega/\tilde{\Delta}}{1 + \left(\Omega/\tilde{\Delta}\right)^2} / \arctan\left(\frac{\Omega}{\tilde{\Delta}}\right) - \frac{1}{4}G, \end{aligned} \tag{20}$$

Here $\tilde{g}$ is the average single-particle level density and $\tilde{\Delta}$ the average paring gap corresponding to a pairing strength G

$$\tilde{\Delta} = 2\Omega \exp\left(-\frac{1}{G\tilde{g}}\right), \tag{21}$$

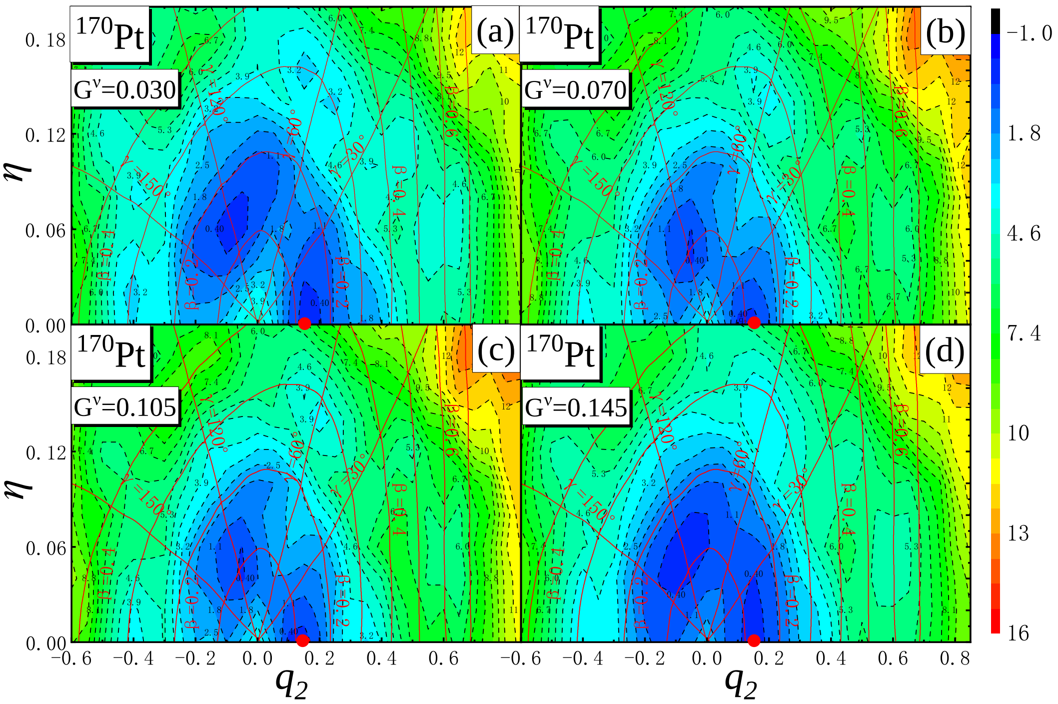

Fig. 2. Potential energy surface of ^{170}Pt projected onto the (q_2, η) plane under different pairing interaction strengths G^{ν} (MeV), while the proton pairing interaction strength is fixed at $G^{\pi} = 0.100$ MeV. The energy is minimized in the q_4 direction and q_3 is set to 0 and normalized to zero energy at the ground-state value. The ground-state deformation is represented by a red dot.

D. Influence of Pairing Interactions on the Shape Coexistence of ^{170}Pt, ^{172}Hg and ^{174}Pb Isotopes

Figure 2 shows the PES of ^{170}Pt projected onto the (q_2, η) plane for different pairing interaction strengths G^{ν} (MeV), while the proton pairing interaction strength is fixed at $G^{\pi} = 0.100$ MeV. G^{ν} and G^{π} represent the neutron and proton pairing interaction strengths (MeV), respectively. The energy is minimized in the q_4 direction and q_3 is set to 0 and normalized to zero energy at the ground-state value. The choice of G^{ν} varying from 0.03 MeV to 0.145 MeV, and $G^{\pi} = 0.100$ MeV, is based on the fact that our calculations in next section, when employing $G^{\nu} = 0.145$ MeV and $G^{\pi} = 0.100$ MeV, closely matched the experimental odd-even mass differences for the ^{171}Pt to ^{180}Pt isotopes. Therefore, this range was selected to study the effects of pairing strength variation on shape coexistence. The red lines represent the corresponding (β, γ) coordinates, with γ coordinates distributed within $0 \leq \gamma \leq 180°$. The β coordinate values are taken as $0.1, 0.2, \ldots$, etc.

In Figures 2 (a)-(d), the potential energy surface (PES) of ^{170}Pt is shown for different values of the neutron pairing interaction strength G^{ν}, while the proton pairing interaction strength is fixed at $G^{\pi} = 0.100$ MeV. The values of G^{ν} are as follows: 0.030 MeV, 0.070 MeV, 0.105 MeV, and 0.145 MeV. As shown, the ground-state of the ^{170}Pt isotope is located at $(q_2 \approx 0.150, \eta = 0)$, indicating a prolate shape for different pairing strengths. The other minimum at $(q_2 \approx -0.150, \eta = 0.04, \gamma = 120°)$ described in Figures 2 is simply the reflection of the ground state minimum.

It is noteworthy to highlight the existence of two distinct shape isomers in ^{170}Pt for different pairing strengths. The first one is an oblate shape isomer located at $(q_2 = -0.400, \eta = 0)$, with an energy approximately 3.900 MeV above the ground-state. The second one is a triaxial shape isomer at $(q_2 \approx 0.600, \eta \approx 0.060\ (\gamma \approx 10°))$, positioned around 4.0 MeV above the ground-state. These isomers represent local minima on the potential energy surface, separated from the ground-state by energy barriers, highlighting the complex deformation characteristics of the nucleus. with the increase pairing strength, both shape isomers become shallower. When the pairing strength G^{ν} reaches 0.145, the oblate isomer disappears (see Fig. 2 (d)).

Depicted in Figures 3 (a)-(d), the PES for different pairing interaction strengths demonstrates the evolution of the triaxial minimum at $(q_2 = 0.150, \eta = 0.020)$ to the oblate minimum at $(q_2 = 0.100, \eta = 0.040)$ as the pairing interaction strength increases. The nucleus ^{172}Hg is nearly γ-unstable, with the energy difference between different points in the ground-state valley not exceeding approximately 0.4 MeV. Additionally, three shape isomers are visible in the (a)-(d) maps: a prolate isomer at $(q_2 \approx 0.600, \eta = 0)$, $E \approx 5.0$ MeV; a triaxial isomer at $(q_2 \approx 0.400, \eta = 0.100)$, $E \approx 4.0$ MeV, and an oblate one at $(q_2 \approx -0.45, \eta = 0)$, $E \approx 4.0$ MeV. These local minima are separated by energy barriers of approximately 1 MeV in height. As the pairing strength increases, all the shape isomers gradually become shallower, and by $G^{\nu} = 0.145, \mathrm{MeV}$ and $G^{\pi} = 0.100, \mathrm{MeV}$ (Figure 3 (d)), the triaxial isomer at $(q_2 \approx 0.400, \eta = 0.100)$ disappear.

The PES of ^{174}Pb, as presented in Figures 4 (a)-(d), reveals a prolate ground-state $(q_2 \approx 0.150, \eta = 0)$ (in Fig. 4 (a)) tend to become spherical (in Fig. 4 (d))as the pairing interaction strength increases. Particularly interesting are the shape isomers observed here: a prolate shape at $(q_2 = 0.600, \eta = 0, E \approx 5.0, \mathrm{MeV})$ and a slightly triaxial oblate shape at $(q_2 = 0.450, \eta = 0.020, E \approx 3.9, \mathrm{MeV})$ in Fig. 4 (a) and (b). As the pairing strength increases, both shape isomers gradually become shallower, and by $G^{\nu} = 0.145, \mathrm{MeV}$ and $G^{\pi} = 0.100, \mathrm{MeV}$ (Figure 4 (d)), they almost disappear. Overall, regardless of the pairing strength, there is no indication of robust shape coexistence in this nucleus.

Figures 5 illustrate the PES projections of ^{170}Pt, ^{172}Hg, and ^{174}Pb under realistic pairing interaction strengths, $G^{\nu} = 0.145$ MeV and $G^{\pi} = 0.100$ MeV under both Exact and BCS pairing schemes.

As shown in Figure 5, the ground state of ^{170}Pt is prolate, located at $(q_2 = 0.15, \eta = 0)$ under both Exact and BCS pairing schemes. However, BCS pairing exhibits a shallower depth for the prolate minimum compared to Exact pairing, indicating a less pronounced prolate ground state. Furthermore, a triaxial isomer appears located at $(q_2 \approx 0.600, \eta \approx 0.060\ (\gamma \approx 10^{\circ}))$ under Exact pairing, whereas it is less distinguishable in the BCS case.

The ground state of ^{172}Hg (see Fig. 5) is found at $(q_2 = 0.10, \eta \approx 0.04)$ as an oblate minimum, with another minimum at $(q_2 \approx -0.100, \eta \approx 0.02)$, which exhibits γ-unstable deformation. The PES of ^{172}Hg provides an excellent example of a nearly γ-unstable nucleus. Under Exact pairing, this γ-unstable minimum is more symmetric, with clear reflections around $\gamma = 150^{\circ}$, $\gamma = 30^{\circ}$, and $\gamma = 90^{\circ}$. Under BCS pairing, the γ-unstable features are less prominent, and the oblate minimum becomes more dominant. Additionally, two shape isomers are visible Under Exact pairing modle: a prolate isomer at $(q_2 \approx 0.600, \eta = 0)$, $E \approx 4.6$ MeV, and an oblate one at $(q_2 \approx -0.45, \eta = 0)$, $E \approx 4.6$ MeV. However, they are not distinguishable in the BCS case.

As shown in Figures 5 (c), the ground state shape of ^{174}Pb tends to be spherical. The PES under Exact pairing reveals a nearly spherical configuration with minor prolate and oblate shape isomers. In contrast, BCS pairing results in a more pronounced spherical minimum and diminishes the depth of shape isomers.

In summary, as the number of protons increases, the ground state transitions from prolate for ^{170}Pt to the coexistence of γ-unstable and oblate for ^{172}Hg, eventually approaching a nearly spherical configuration for ^{174}Pb. The comparison between Exact and BCS pairing demonstrates that BCS pairing tends to smooth out shape coexistence and reduce the depth of shape isomer, leading to less pronounced deformation features.

E. Shape coexistence analysis in the Pt isotope chain

In this paper, we investigate the potential energy surfaces (PES) of the even-even $^{170-180}$Pt isotopes using the exactly solvable deformed mean-field plus pairing model. Our analysis provides a comprehensive examination of the shape coexistence phenomena across these isotopes.

The pairing interaction strength, denoted as G, serves as the sole adjustable parameter within our model. It is typically determined either through empirical formulas or by fitting to experimental odd-even mass differences [40, 41]. In this study, we precisely determined G^{ν} by fitting the experimental odd-even mass differences for the $^{171-180}$Pt isotope chain and G^{π} by fitting the experimental odd-even mass differences for the ^{174}Pt to ^{178}Pb isotonic chain. The odd-even mass differences were computed using the following expression:

$$P\,(A) = E_{\text{total}}\,(N+1, Z) + E_{\text{total}}\,(N-1, Z) - 2E_{\text{total}}\,(N, Z)\,, \tag{3.2}$$

This quantity is highly sensitive to variations in the pairing interaction strength G [42], due to the pairing interaction between nucleons. As shown in Fig. 6, by employing $G^{\nu} = 0.145$ MeV and $G^{\pi} = 0.100$ MeV, our calculations closely reproduced the experimental odd-even mass differences for the $^{171-180}$Pt isotopes, yielding a root mean square deviation of $\sigma = 0.465$ MeV. Additionally, as display in Fig. 7 for the ^{174}Pt to ^{178}Pb isotonic chain, the calculations closely matched the experimental odd-even mass differences, with a root mean square deviation of $\sigma = 1.192$ MeV.

$$\sigma = \sqrt{\sum_{\mu=1}^{\mathcal{N}} \left(P_{\mu}^{\text{Theor.}} - P_{\mu}^{\text{Expt.}}\right)^2 / \mathcal{N}}, \tag{3.3}$$

Here, $P_{\mu}^{\text{Theor.}}$ and $P_{\mu}^{\text{Expt.}}$ represent the theoretical and experimental values of the odd-even mass differences, respectively, and $\mathcal{N}$ denotes the total number of data points.

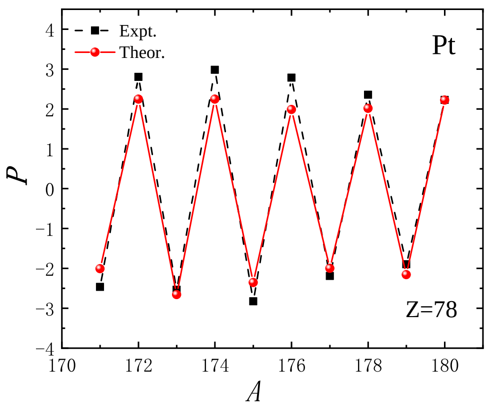

Fig. 6. Odd-even mass differences (in MeV) for Pt isotopes. "Expt." represents experimental values, and "Theor." represents theoretical values. Experimental data are from [42].

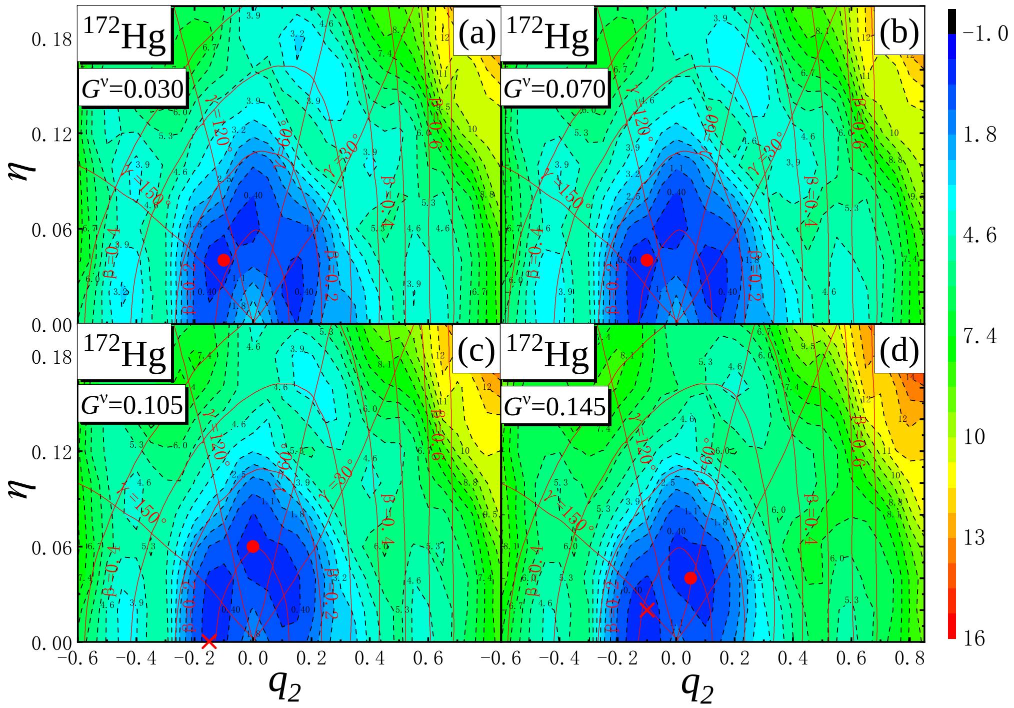

Fig. 3. Potential energy surface of ^{172}Hg projected on the (q_2, η) plane with variation of neutron pairing interaction strengths G^{ν} (MeV), while the proton pairing interaction strength is fixed at $G^{\pi} = 0.100$ MeV. The energy is minimized in the q_4 direction and q_3 is set to 0 and normalized to zero energy at the ground-state value. The ground-state deformation is represented by a red dot, while the coexistence minimum is indicated by a red cross.

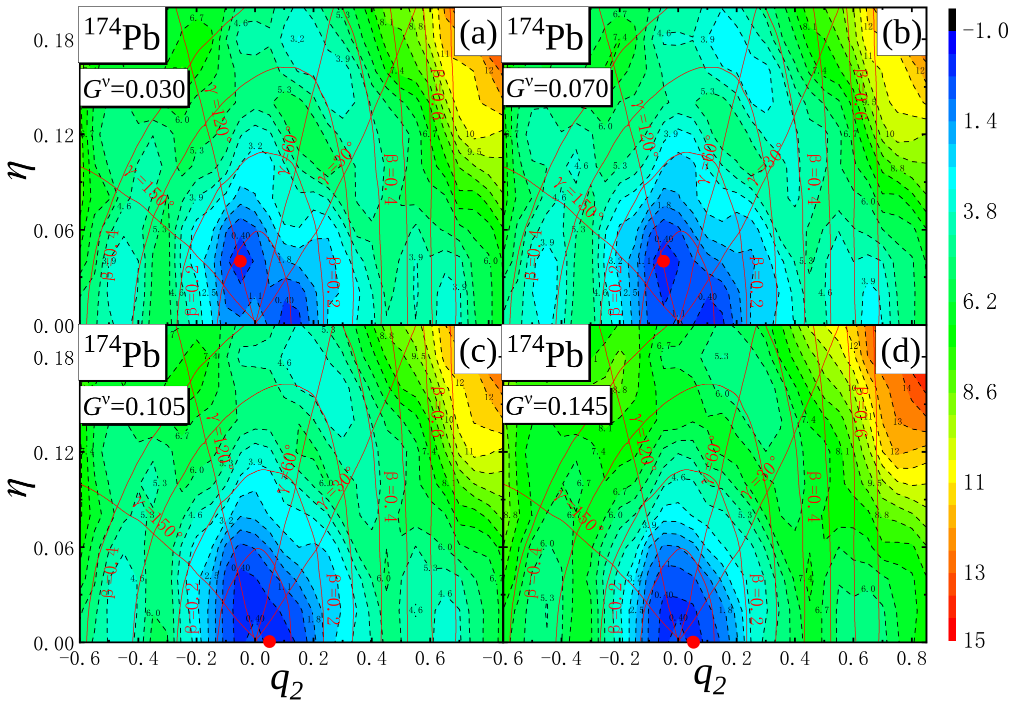

Fig. 4. Potential energy surface of ^{174}Pb projected onto the (q_2, η) plane under different pairing interaction strengths G^{ν} (MeV), while the proton pairing interaction strength is fixed at $G^{\pi} = 0.100$ MeV. The energy is minimized in the q_4 direction and q_3 is set to 0 and normalized to zero energy at the ground-state value. The ground-state deformation is represented by a red dot.

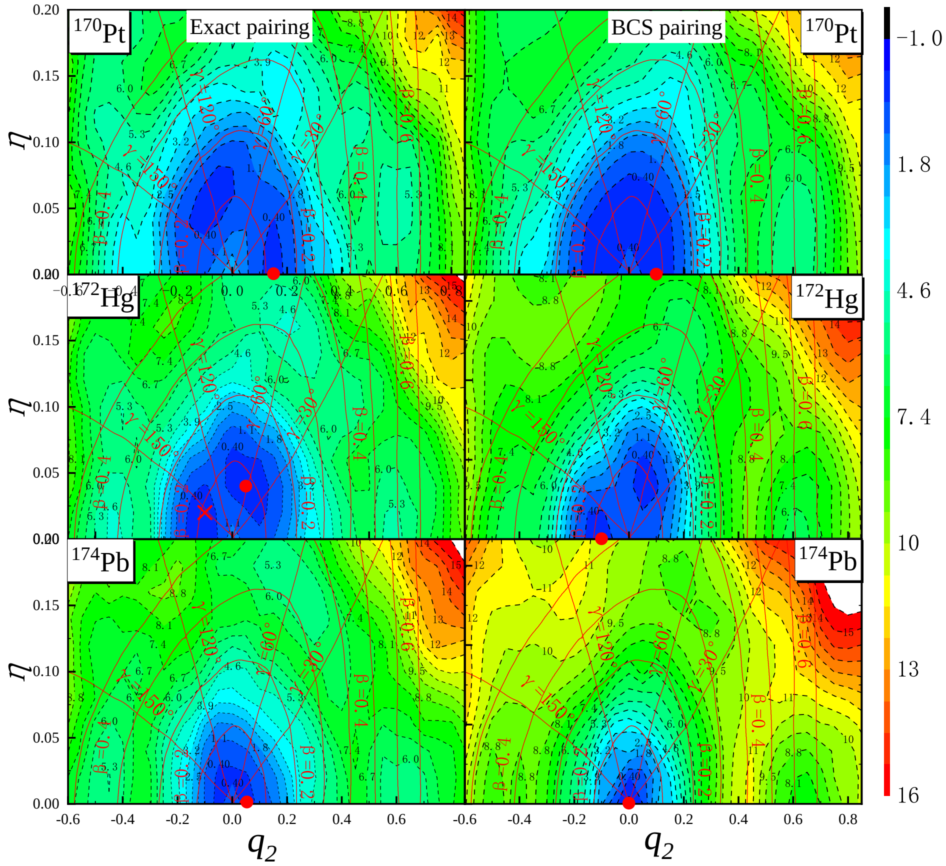

Fig. 5. Potential energy surfaces of ^{170}Pt, ^{172}Hg and ^{174}Pb projected on the (q_2, η) plane under both Exact and BCS pairing schemes, with the energy minimized in the q_4 direction, q_3 set to 0 and normalized to zero energy at the ground-state value. The realistic pairing interaction strengths $G^{\nu} = 0.145,$ MeV and $G^{\pi} = 0.100$ MeV are adopted.

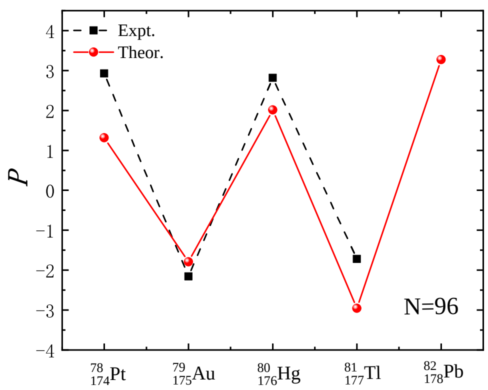

Fig. 7. Odd-even mass differences (in MeV) for the ^{174}Pt to ^{178}Pb isotonic chain. "Expt." represents experimental values, and "Theor." represents theoretical values. Experimental data are from [42].

Next, we examine the PES of the $^{170-180}$Pt even-even isotopes under the determined pairing interaction strengths $G^{\nu} = 0.145$ MeV and $G^{\pi} = 0.100$ MeV. Figure 8 shows the PES projected onto the (q_2, η) plane. For the ^{170}Pt, the ground-state exhibits a prolate deformation at ($q_2 = 0.15, \eta = 0$). In contrast, for ^{172}Pt, a more deformed minimum emerges, leading to the coexistence of a triaxial shape ($\gamma \approx 30°$) and a nearly prolate-deformed minimum at ($\gamma \approx 120°$), indicative of γ-unstability due to the presence of multiple low-energy configurations at different γ values. The triaxial shape is even more pronounced in ^{174}Pt, where the ground-state is triaxial with deformation parameters ($q_2 = 0.020, \eta = 0.10$, $\beta \approx 0.2, \gamma \approx 90°$)) and coexisting a prolate minimum at ($q_2 = 0.15, \eta = 0$). In ^{176}Pt a γ -unstable ground-state and a prolate minimum coexist, but by ^{178}Pt and ^{180}Pt, a well-deformed prolate minimum quickly develops, becoming the most pronounced prolate ground-state at the mid-shell.

The findings from this work are broadly consistent with the results in Ref. [43], which studied $^{172-194}$Pt isotopic chain in the framework of the interacting boson model and self-consistent Hartree-Fock-Bogoliubov calculation using the Gogny-D1S interaction. Both studies identify the shape coexistence in the $^{172-176}$Pt region, with the γ-unstable minima and triaxial shapes in ^{174}Pt. Additionally, both works show the dominance of prolate deformation in ^{178}Pt and ^{180}Pt, with the prolate minimum becoming the most pronounced ground state at mid-shell.

It is noteworthy that a triaxial shape isomer exists for $^{170-174}$Pt, characterized by ($q_2 \approx 0.600, \eta \approx 0.060$ $(\gamma \approx 10°)$), and positioned approximately 5.0MeV above the ground-state. However, this triaxial shape isomer vanishes for $^{176-180}$Pt.

III. CONCLUSION

In this study, we have systematically investigated the shape coexistence phenomenon in isotopes near the magic proton number $Z = 82$, focusing specifically on the nuclei ^{170}Pt, ^{172}Hg, and ^{174}Pb, as well as the Pt isotopic chain from ^{170}Pt to ^{180}Pt. Our analysis, using a macroscopic-microscopic approach that combines the Lublin-Strasbourg Drop model with a Yukawa-Folded potential and pairing corrections, reveals significant insights into the impact of pairing interactions on nuclear shape evolution.

The PES of $^{170}\mathrm{Pt}$ reveals a prolate ground state with additional triaxial and oblate shape isomers. Both shape isomers become progressively shallower with increasing neutron pairing strength (G^{ν}), and the oblate isomer vanishes at $G^{\nu} = 0.145$ MeV, indicating a significant dependence of shape isomers on pairing strength. The ground-state deformation of $^{172}\mathrm{Hg}$ transitions from triaxial to oblate with increasing G^{ν}, reflecting its nearly γ-unstable nature. Three shape isomers (prolate, triaxial, and oblate) are observed, with energy barriers separating these configurations. As G^{ν} increases, the triaxial isomer disappears at $G^{\nu} = 0.145$ MeV, demonstrating the impact of pairing interactions on shape stability. $^{174}\mathrm{Pb}$ exhibits a prolate ground state that becomes increasingly spherical with stronger pairing interactions. While shape isomers are present at weaker pairing strengths, their prominence diminishes significantly, and robust shape coexistence is not observed in this nucleus.

For realistic pairing interaction, the ground-state shapes transition from prolate in $^{170}\mathrm{Pt}$ to a coexistence of γ-unstable and oblate shapes in $^{172}\mathrm{Hg}$, ultimately approaching spherical symmetry in $^{174}\mathrm{Pb}$. This progression highlights the interplay between proton number and pairing interactions in shaping nuclear deformation. The comparison between Exact and BCS pairing for realistic ^{170}Pt, ^{172}Hg, and ^{174}Pb demonstrates that BCS pairing tends to smooth out shape coexistence and reduce the depth of shape isomers, leading to less pronounced deformation features.

These findings emphasize the critical role of pairing interactions in shaping nuclear deformation landscapes and shape coexistence, offering deeper insights into the structural evolution of nuclei near the mid-shell region. This study contributes valuable theoretical perspectives to the understanding of nuclear shape phenomena and the influence of pairing interactions on nuclear dynamics.

Based on the analysis of the potential energy surfaces (PES) for the even-even $^{170-180}$Pt isotopes, the results show significant shape evolution across the isotopic chain. In the case of ^{170}Pt, the ground-state exhibits a prolate deformation, with deformation parameters. However, for ^{172}Pt, a more deformed minimum emerges, leading to the coexistence of a triaxial shape and a nearly prolate-deformed minimum at. The triaxial shape becomes even more pronounced in ^{174}Pt, where the ground-state is triaxial with deformation parameters, coexisting with a prolate minimum. For ^{176}Pt, a γ-unstable ground-state coexists with a prolate minimum. By ^{178}Pt and ^{180}Pt, a well-deformed prolate minimum develops rapidly, becoming the most pronounced prolate ground-state at mid-shell.

These results highlight the complex shape evolution in the Pt isotopes, with shape coexistence and γ-unstability playing significant roles in the nuclear structure evolution, particularly around the mid-shell region where prolate deformation dominates.

[1] K. Heyde, and J. L. Wood, Publisher's Note: Shape coexistence in atomic nuclei. Rev. Mod. Phys. **83**,1467 (2011). doi:http://dx.doi.org/10.1103/RevModPhys.83.1655.

[2] H. Morinaga, Interpretation of Some of the Excited States of $4n$ Self-Conjugate Nuclei. Phys. Rev. **101(1)**:254(1956). doi: https://doi.org/10.1103/PhysRev.101.254.

[3] P. Möller, A. J. Sierk, R. Bengtsson et al., Global Calculation of Nuclear Shape Isomers. Phys. Rev. Lett. **103(21)**:212501 (2009). doi: 10.1103/PhysRevLett.103.212501.

[4] M. Siciliano, I. Zanon, A. Goasduff et al., Shape coexistence in the neutron-deficient ^{188}Hg investigated via lifetime measurements. Phys. Rev. C. **102**, 014318 (2020). doi: https://doi.org/10.1103/PhysRevC.102.014318.

[5] R. Julin, T. Grahn, J. Pakarinen et al., In-beam spectroscopic studies of shape coexistence and collectivity in the neutron-deficient Z $\approx$ 82 nuclei. J. Phys. G .**43**, 024004 (2016). doi: 10.1088/0954-3899/43/2/024004.

[6] M. Bender, P. H. Heenen, and P. G. Reinhard, Self-consistent mean-field models for nuclear structure. Rev. Mod. Phys. **75**, 121 (2003). doi: https://doi.org/10.1103/RevModPhys.75.121.

[7] T. Nikšić, D. Vretenar, P. Ring et al., Shape coexistence in the relativistic Hartree-Bogoliubov approach. Phys. Rev. C. **65**, 054320 (2002). doi: https://doi.org/10.1103/Phys Rev C.65.054320.

[8] F. Z. Xing, J. P. Cui , Y. H. Gao et al., Structure and α Decay of Superheavy Nucleus ^{296}Og. Nucl. Phys. Rev. **40** (4):511-518 (2023). doi: 10.11804/NuclPhysRev.40.2023059.

[9] J. Bardeen, L. N. Cooper, and J. R. Schrieffer, Theory of Superconductivity. Phys. Rev. **108**, 1175 (1957). doi: https://doi.org/10.1103/PhysRev.108.1175.

[10] A. Bohr, B. R. Mottelson, and D. Pines, Possible Analogy between the Excitation Spectra of Nuclei and Those of the Superconducting Metallic State. Phys. Rev. 110(4):936-938 (1958). doi: https://doi.org/10.1103/PhysRev.110.936.

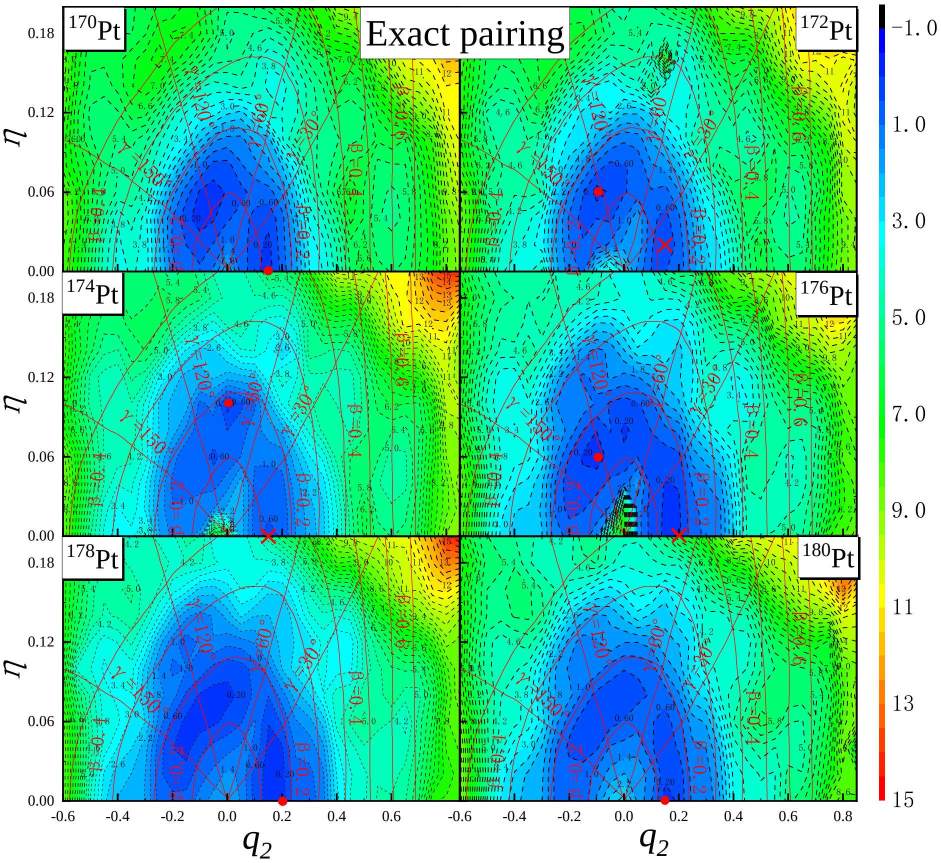

Fig. 8. A potential energy surfaces of the $^{170-180}$Pt even-even isotopes chain, projected on the (q_2, η) plane using the exact pairing model, where the energy is minimized in the q_4 direction with q_3 set to 0, with neutron and proton pairing interaction strengths of $G^{\nu} = 0.145$ MeV, $G^{\pi} = 0.100$ MeV. The ground-state deformation is represented by a red dot, while the coexistence minimum is indicated by a red cross.

[11] S. T. Belyaev, Effect of pairing correlations on nuclear properties. Dan. Mat. Fys. Medd. **31**, 11 (1959). doi:https://www.osti.gov/biblio/4262925.

[12] Y. Z. Wang, F. Z. Xing, J. P. Cui et al., Roles of tensor force and pairing correlation in two-proton radioactivity of halo nuclei. Chinese Physics C Vol. **47**, No. 8, 084101 (2023). doi: 10.1088/1674-1137/acd680.

[13] N. Sandulescu, and G. F. Bertsch, Accuracy of BCS-based approximations for pairing in small Fermi systems nuclei. Phys. Rev. C. **78**, 064318 (2008). doi: http: //doi. org/10. 1103/PhysRevC. 78. 064318.

[14] I. Talmi, Simple Models of Complex Nuclei. (Harwood Academic Publishers, Switzerland). (1993). doi: https: //doi. org/10. 1201/9780203739716.

[15] R. W. Richardson, A restricted class of exact eigenstates of the pairing-force Hamiltonian. Phys. Lett. **3**, 3277 (1963). doi: https: //doi. org/10. 1016/0031-9163(63)90259-2; Application to the exact theory of the pairing model to some even isotopes of lead. Phys. Lett. **5**, 82 (1963). doi: https: //doi. org/10. 1016/S0375-9601(63)80039-0; R. W. Richardson and N. Sherman, Exact eigenstates of the pairing-force Hamiltonian. Nucl. Phys. **52**, 221 (1964). doi: https: //doi. org/10. 1016/0029-5582(64)90687-X; Pairing models of Pb^{206}, Pb^{204} and Pb^{202}. Nucl. Phys. **52**, 253 (1964). doi: https://doi.org/10.1016/0029-5582(64)90690-X.

[16] M. Gaudin, Diagonalization of a class of spin Hamiltonians. Phys. J. **37**, 1087 (1976). doi: https://www. osti. gov/etdeweb/biblio/7120011

[17] F. Pan, J. P. Draayer, and W. E. Ormand, A particle-number-conserving solution to the generalized pairing problem. Phys. Lett. B. **422**, 1 (1998). doi: https://doi.org/10.1016/S0370-2693(98)00034-3.

[18] J. Dukelsky, C. Esebbag, and S. Pittel, Electrostatic mapping of nuclear pairing. Phys. Rev. Lett. **88**, 062501 (2002). doi: https: //doi. org/10. 1103/PhysRevLett. 88. 062501; J. Dukelsky, S. Pittel, G. Sierra, Colloquium: Exactly solvable Richardson-Gaudin models for many-body quantum systems. Rev. Mod. Phys. **76**, 643 (2004). doi: https: //doi. org/10. 1103/RevModPhys. 76. 643.

[19] X. Guan, K. D. Launey, M. X. Xie et al., Heine-Stieltjes correspondence and the polynomial approach to the standard pairing problem. Phys. Rev. C **86**,024313 (2012). doi: https: //doi. org/10. 1103/PhysRevC. 86. 024313.

[20] A. Faribault, O. E. Araby, C. Sträter et al., Gaudin models solver based on the correspondence between Bethe ansatz

and ordinary differential equations. Phys. Rev. B **83**, 235124 (2011). doi: https://doi.org/10.1103/PhysRevB.83.235124; O. El Araby, V. Gritsev, and A. Faribault, Bethe ansatz and ordinary differential equation correspondence for degenerate Gaudin models. Phys. Rev. B **85**, 115130 (2012). doi: https://doi.org/10.1103/PhysRevB.85.115130.

[21] X. Guan, K. D. Launey, M. X. Xie et al., Numerical algorithm for the standard pairing problem based on the Heine-Stieltjes correspondence and the polynomial approach. Comp. Phys. Commun. **185**, 2714 (2014). doi:https://doi.org/10.1016/j.cpc.2014.05.023.

[22] C. Qi and T. Chen, Exact solution of the pairing problem for spherical and deformed systems. Phys. Rev. C **92**, 051304(R) (2015). doi: 10.1103/PhysRevC.92.051304

[23] X. Guan, H. C. Xu, F. Pan et al., Ground state phase transition in the Nilsson mean-field plus standard pairing model. Phys. Rev. C **94**, 024309 (2016). doi:https: // doi. org / 10. 1103 / PhysRevC . 94 . 024309 .

[24] X. Guan and C. Qi, An iterative approach for the exact solution of the pairing Hamiltonian. Comp. Phys. Comm. **275**, 108310 (2022). doi: https: //doi. org/10. 1016/j. cpc. 2022. 108310.

[25] X. Guan, Y. Xin, Y. J. Chen et al.,Impact of pairing interactions on fission in the deformed mean-field plus standard pairing model. Phys. Rev. C **104**, 044329 (2021). doi: https: //doi. org/10. 1103/PhysRevC. 104. 044329.

[26] X. Guan, T. C. Wang, W. Q. Jiang et al.,Impact of the pairing interaction on fission of U isotopes. Phys. Rev. C **107**, 034307 (2023). doi: https: //doi. org/10. 1103/PhysRevC. 107. 034307.

[27] X. Guan, J. H. Zheng, and M. Y. Zheng, Pairing effects on the fragment mass distribution of Th, U, Pu, and Cm isotopes. Nucl. Sci. Tech. **34**, 173 (2023). doi: 10. 1007/s41365-023-01316-x.

[28] K. Pomorski, B. Nerlo-Pomorska, A. Dobrowolski, et al. Shape isomers in Pt, Hg and Pb isotopes with $N \leq 126$. Eur. Phys. J. A, **56**, 107 (2020).doi: 10. 1140/epja/s10050-020-00115-x.

[29] C. Schmitt, K. Pomorski, B. K. Nerlo-Pomorska et al., Performance of the Fourier shape parametrization for the fission process. Phys.Rev.C **95**, 034612 (2017). doi: 10.1103/PhysRevC.95.034612.

[30] K. Pomorski, J. M. Blanco, P. V. Kostryukov et al., Fission fragment mass yields of Th to Rf even-even nuclei. Chin. Phys. C **45** 054109 (2021). doi: 10.1088/1674-1137/abec69.

[31] L. L. Liu, Y. J. Chen, X. Z. Wu et al., Analysis of nuclear fission properties with the Langevin approach in Fourier shape parametrization. Phys.Rev. C **103**, 044601 (2021). doi: 10.1103/PhysRevC.103.044601.

[32] A. Bohr, The coupling of nuclear surface oscillations to the motion of individual nucleons. Dan. Mat. Fys. Medd. **26**, 14 (1952).

[33] T. Kaniowska, A. Sobiczewski, K. Pomorski et al., Microscopic inertial functions for nuclei in the barium region.Nucl. Phys. A **274**, 151 (1976). doi: https://doi. org/10. 1016/0375-9474(76)90233-5.

[34] S. G. Rohoziáski,and A. Sobiczewski, Hexadecapole Nuclear Potential for Non-Axial Shapes, Acta Phys. Pol. B **12**, 1001 (1981). doi: 10. 1016/0003-4916(82)90273-1.

[35] P. Möller, A .J. Sierk, R. Bengtsson et al., Atom. Data Nucl. Data Tables **98**, 149, (2012). doi:10. 1103/PhysRevC. 79. 064304.

[36] K. Pomorski ,and J. Dudek,Nuclear liquid-drop model and surface-curvature effects. Phys. Rev. C **67**, 044316 (2003). doi: 10. 1103/PhysRevC. 67. 044316.

[37] V. M. Strutinsky,Shell effects in nuclear masses and deformation energies. Nucl. Phys. A **95**, 420 (1967). doi: 10. 1016/0375-9474(67)90510-6.

[38] V. M. Strutinsky,'Shells' in deformed nuclei Nucl. Phys. A **122**, 1 (1968). doi: 10. 1016/0375-9474(68)90699-4.

[39] S. G. Nilsson, C. F. Tsang, A. Sobiczewski, et al. On the nuclear structure and stability of heavy and superheavy elements. Nucl. Phys. A. **95**, 1 (1969). doi: 10. 1016/0375-9474(69)90809-4.

[40] Y. Sun, Projection techniques to approach the nuclear many-body problem.Phys. Scr. **91**, 043005 (2016). doi: 10. 1088/0031-8949/91/4/043005.

[41] M. Bender, K. Rutz, P.-G. Reinhard et al.,Pairing gaps from nuclear mean-fieldmo dels. Eur. Phys. J. A **8**, 59 (2000). doi: 10. 1007/s10050-000-4504-z.

[42] U. S. National Nuclear Data Center: http://www.nndc.bnl.gov/.

[43] J. E. García-Ramos, K. Heyde, L. M. Robledo et al.,Shape evolution and shape coexistence in Pt isotopes: Comparing interacting boson model configuration mixing and Gogny mean-field energy surfaces. Phys.Rev.C **98**, 034313 (2014). doi: 10. 1103/PhysRevC. 81. 024310.